applied sciences

MDPI

Article

Influence of Loess–Mudstone Strata Structure on Slope Seismic Stability of Loess Plateau in China

Zhaopeng Zhang [1,2,*], Wenhao Qi [1], Zhiyi Zhao [2] and Tong Zheng [1]

[1] Key Laboratory of Earthquake Engineering and Engineering Vibration, Institute of Engineering Mechanics, China Earthquake Administration, Harbin 150080, China
[2] School of Environment and Safety Engineering, North University of China, Taiyuan 030051, China
* Correspondence: jidazhangzhaopeng@126.com; Tel.: +86-150-7668-4659

Abstract: The widely distributed loess–mudstone strata structure in the Loess Plateau of China is one of the fundamental reasons for the susceptibility and group occurrence of seismic landslides in the area. This study took the loess landslides induced by the Haiyuan earthquake as a case study. Through extensive field investigations, the loess cover thickness, mudstone dip angle, slope height, and slope angle were chosen as the influencing factors. Together with mathematical statistics and geotechnical tests, two models, one of a loess–mudstone slope and the other of a pure loess slope, were constructed. Their seismic stabilities under different slope angles and slope heights were compared to analyze the influence of the underlying mudstone strata on the loess slope seismic stability. Meanwhile, a sensitivity analysis of these strata factors affecting the seismic stability of the loess–mudstone slope was carried out based on the orthogonal test. The results showed that ignoring the underlying mudstone strata would lead to smaller calculation results than the actual situation. The sensitivity influence of the factors on the loess–mudstone slope seismic stability comprised the slope angle, loess cover thickness, slope height, and mudstone dip angle from high to low.

Keywords: loess slope; strata structure; sensitivity analysis; stability analysis

check for updates

Citation: Zhang, Z.; Qi, W.; Zhao, Z.; Zheng, T. Influence of Loess–Mudstone Strata Structure on Slope Seismic Stability of Loess Plateau in China. *Appl. Sci.* **2023**, *13*, 12854. https://doi.org/10.3390/app132312854

Received: 25 September 2023
Revised: 27 November 2023
Accepted: 27 November 2023
Published: 30 November 2023

Copyright: © 2023 by the authors. Licensee MDPI, Basel, Switzerland. This article is an open access article distributed under the terms and conditions of the Creative Commons Attribution (CC BY) license (https://creativecommons.org/licenses/by/4.0/).

1. Introduction

Loess is a special soil that accounts for approximately 10% of the total coverage area of soil, with a wide global distribution [1]. Due to its unique characteristics, such as aerial pores, weak cementation structure, and collapsibility [2], it is easily destroyed when subjected to strong earthquakes, leading to a large number of loess landslides and resulting in serious casualties and property losses. At the same time, loess areas are often areas with frequent earthquakes; for example, the Loess Plateau, the largest loess distribution area in the world, is an earthquake-prone area. Historically, six violent earthquakes of magnitude M > 8.0 have been recorded here [3], providing a large number of cases for the study of loess seismic landslides. In 2017, loess was identified as a challenging soil by the International Technical Committee on Earthquake Geotechnical Engineering. Therefore, it is imperative to explore the formation rules of loess seismic landslides to reduce the disaster impact.

Research interest in loess seismic landslide disasters began with Close et al.'s [4] field investigation of loess landslides induced by the Haiyuan earthquake. Since then, investigation and statistical analyses have been some of the main methods of studying loess seismic landslides, specifically the topographic conditions, geomorphic characteristics, geological structures, disaster range, and seismic parameters of typical loess landslides in different intensity regions. Various researchers have summarized the classification of the landslides [5,6], analyzed the basic characteristics of landslide distribution [7], refined the understanding of the ideal geological conditions for the formation of landslides, and determined the maximum sliding distance [8]. These provided basic information for the study of the failure process and risk assessment of landslides induced by earthquakes.

In addition, the improvement of satellite remote sensing image resolution and the wide application of unmanned aerial vehicle (UAV) low-altitude photogrammetry have provided great convenience for landslide investigations; compared to field investigations, these methods can quickly analyze the number and distribution of landslides [9]. Sato et al. [10], Gorum et al. [11], Zhang et al. [12], and Chang [13] carried out significant works on the spatial distribution characteristics and development models of seismic landslides using these technologies.

In recent years, the use of geotechnical tests and numerical simulations to study seismic landslides has become an interesting approach [14]. These methods also support field investigations and have been widely used to analyze the liquefaction behavior and dynamic properties of loess [15–18], to study the dynamic response and macroscopic deformation and failure process of loess slopes [19–25], and, thus, revealed the formation mechanism of loess seismic landslides. Currently, some good results have been achieved, especially in the study of one particular landslide. For example, using the Hilbert–Huang transform (HHT) to transform nonlinear and nonstationary seismic records into Hilbert spectra, the instantaneous frequency energy of the loess layer and mudstone layer of the Buzi landslide were compared in terms of time–frequency–energy, and the landslide failure process was studied from an energy perspective [26]. Based on the discrete element theory, landslide models were established using the particle flow code (PFC), and the dynamic responses and motion characteristics of landslides were studied by simulating the motion and interaction between particles under seismic conditions [27,28].

It can be seen that there are few studies on the impact of strata structure on loess seismic landslides at present, and most of them are aimed at the dynamic response and failure modes of one particular landslide, whereas a loess seismic landslide often has characteristics of clustering, for example, more than 7000 loess landslides were triggered by the 1920 Haiyuan earthquake [29]. At the same time, the loess–mudstone strata structure is widely developed in the Loess Plateau, and this kind of strata structure often causes the loess to slide along the underlying mudstone during earthquakes; loess–mudstone landslides formed thereby are widely distributed and frequently develop in this area [30], whereas conclusions based on one particular landslide have certain limitations. In view of this, the high-intensity area of the Haiyuan earthquake was selected as the study area in this paper. Through field investigations of existing landslides, the topographic conditions (e.g., the original slope height, slope angle, and slope shape) of these landslides were statistically analyzed and the physical and mechanical parameters of loess were obtained through geotechnical tests. Combined with the pseudostatic method and taking safety factors as the evaluation index, the influence model of the underlying strata structure on the seismic stability of a loess slope was evaluated. Further, based on orthogonal tests and a range analysis, a sensitivity analysis was carried out for four factors affecting the loess slope seismic stability, i.e., the slope height, slope angle, loess cover thickness, and underlying mudstone dip angle. The results provide a scientific reference and theoretical basis for reasonably evaluating the seismic stability of loess slopes and optimizing the antiseismic design of loess slopes.

2. Materials and Methods

The Haiyuan earthquake is one of the largest earthquakes recorded in the history of China. It is among the world's biggest earthquakes, with a magnitude of 8.5 and a macroseismic intensity of XII [31]. It is located in a hilly area of loess geomorphology. Thousands of loess landslides have been induced in Xiji and Haiyuan seismic areas. Although the earthquake occurred over 100 years ago, most landslides in this area are well preserved due to low precipitation and no other external damage, making it a natural site for loess seismic landslide studies. For example, Figure 1 shows the Shenjiazui landslide located in Guyuan city, including the crown, main scarp, flank, and toe of the landslide. However, due to the particular characteristics of loess, knowledge of the strata structure complexity [32] and

its distribution has remained relatively underdeveloped. Although the earthquake caused many loess landslides, a systematic study was not started until the 1990s [33–35].

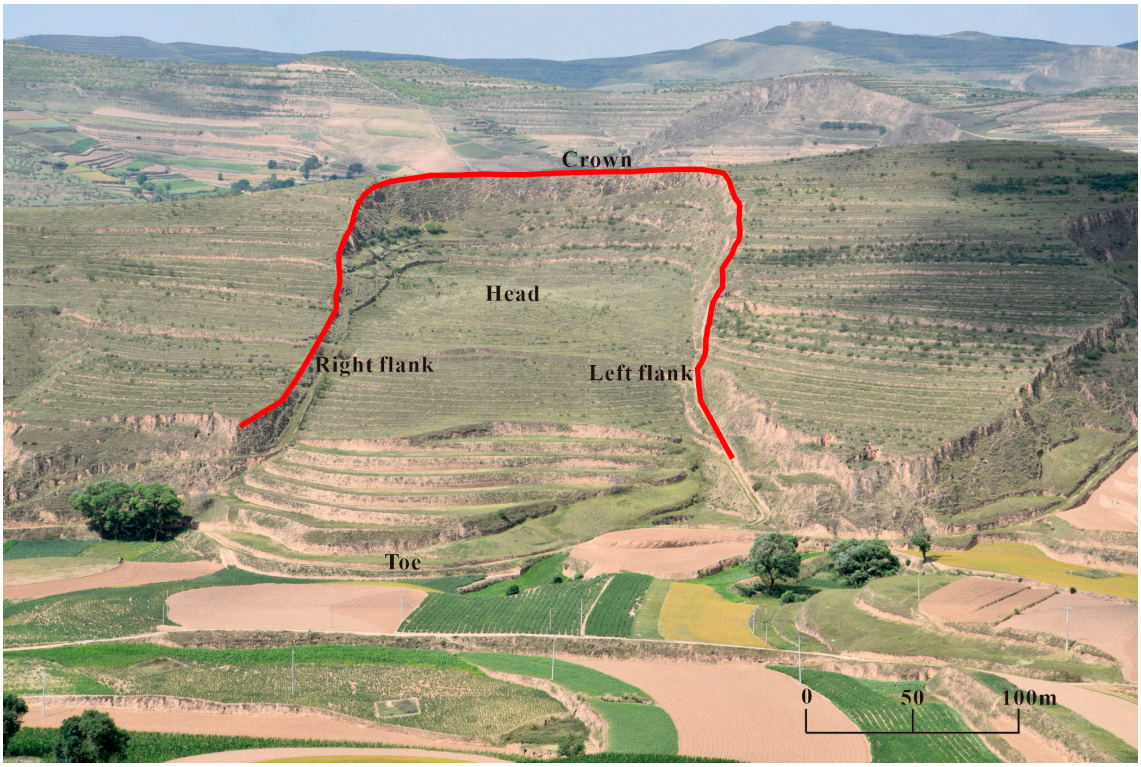


Figure 1. Shenjiazui landslide (E 105.4867°, N 35.8803°). The landslide is 90 km away from the epicenter. It has a length of approximately 300 m, a width of approximately 250 m, and a volume of approximately 9.6 million m^3; the main sliding direction is 65°, and the slope angle of the landslide body is 10°.

2.1. Site Selection

This paper took the concentrated areas of loess landslides induced by the Haiyuan earthquake (e.g., Xiji county, Haiyuan county, Jingning county) as the study area. Through years of field investigations, a total of 569 landslides were investigated (as shown in Figure 2). The field investigation mainly used GPS, geological compasses, and laser rangefinders to obtain the geographical location, geometric parameters, and topography of the landslides, and the strata structure and geotechnical characteristics of some typical landslides (Subao landslide, Xinzhuang landslide, etc.) were explored by means of drilling and shear wave velocity testing. Loess seismic landslides in the region were primarily developed in low/gentle loess hilly areas, and the strata generally presented a loess–mudstone dual structure, as shown in Figure 3. Loess is late Pleistocene loess, while the mudstone is Tertiary red mudstone. The dip angle was concentrated between 25° and 30° [36]. Due to the landslides' apparent differences in physical and mechanical properties, most of their contact surfaces constituted the sliding surface of the landslide mass (as shown in Figure 4).

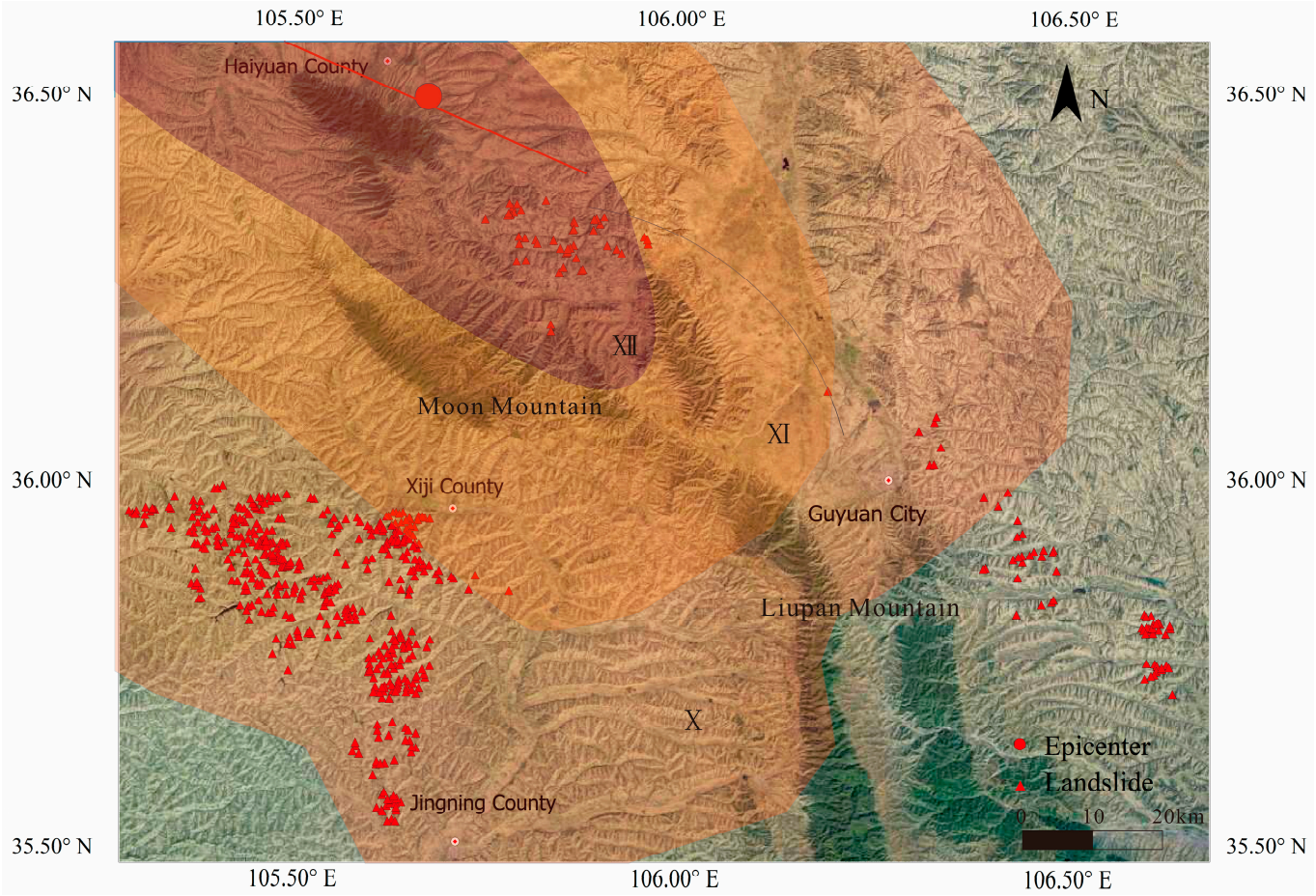


Figure 2. Distribution map of landslides in the study area.

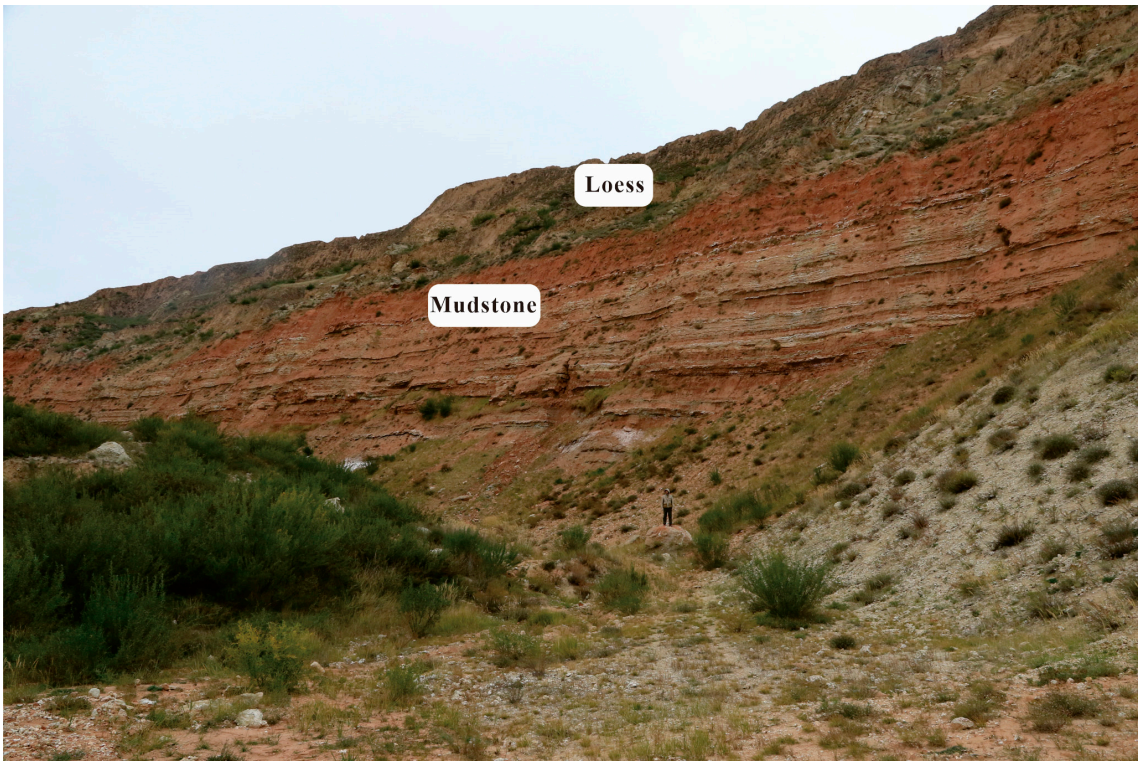


Figure 3. Diagram of strata structure (E 105.858°, N 36.202°).

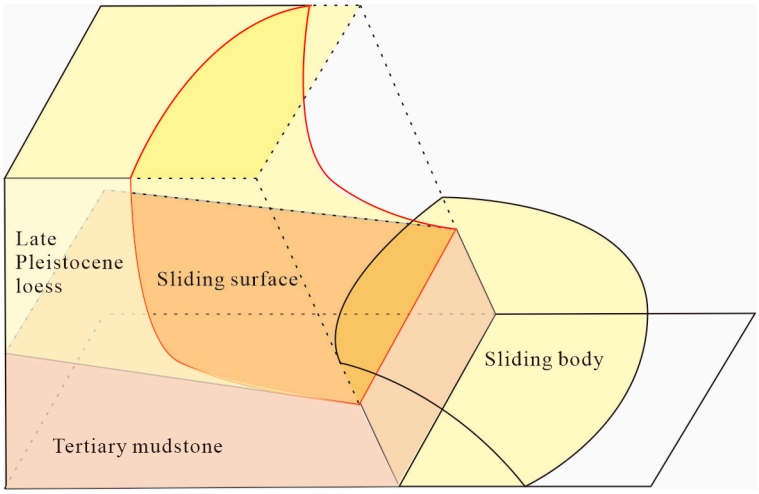


Figure 4. Simplified diagram of sliding mode of loess–mudstone slope.

2.2. Sampling

Borehole sampling was carried out on the SuBao landslide (E 105.858°, N 36.202°) located in Xiji county, as shown in Figures 5 and 6. Through a field investigation, we found that the landslide belonged to a typical loess–mudstone strata structure with a slope height of 160 m, a slope angle of 18 °, and a loess cover thickness of 30 m. It can be seen from Figure 5 that the sliding mass was relatively flat and adjacent to SuBao village, making it easy for drilling machinery transportation and construction. Three boreholes were arranged along the main sliding direction on the sliding mass, with a depth of 2 m below the underlying mudstone layer. The layout and field records of the boreholes can be found in the literature [27].



Figure 5. SuBao landslide.



(**a**) (**b**)

Figure 6. Sampling: (**a**) drilling; (**b**) samples.

2.3. Geotechnical Tests

The geotechnical tests, that is, the direct shear test and the consolidation test, were conducted on undisturbed loess samples obtained from boreholes, as shown in Figure 7. In order to avoid the influence of the loading rate and other factors on the physical and mechanical parameters of the loess samples [37,38], the geotechnical tests in this paper were mainly based on the "Standards for Geotechnical Testing Method" [39]. The density test adopted the cutting ring method and we conducted two parallel tests with an error of less than 0.03 g/cm^3 in the two test results. The consolidation test evaluated the compressibility of loess based on the compression coefficient when the pressure increased from 100 kpa to 200 kpa. The direct shear test used four similar loess samples with vertical stresses of 50 kpa, 100 kpa, 200 kpa, and 300 kpa; shear forces were applied under different vertical stresses and strength parameters, such as the internal friction angle and cohesion, were determined according to Coulomb's law.



(**a**) (**b**)

Figure 7. Geotechnical test: (**a**) consolidation test; (**b**) direct shear test.

2.4. Methods

The pseudostatic method, Newmark method, and time–history analysis method are the three main methods used for analyzing the seismic stability of slopes. Since the Haiyuan earthquake occurred many years ago, the complete seismic wave was not recorded, and the magnitude was too large. The pseudostatic method was used to simplify the seismic

load in this paper. The influence mechanism and model of the strata structure on the loess slope seismic stability were studied.

The pseudostatic method was first introduced into the slope seismic stability analysis by Terzaghi [40]. Due to its clear concept, simplicity, and applicability, researchers have widely adopted it and incorporated it into corresponding specifications [41,42]. Its basic principle is to simplify the instantaneous seismic load to equivalent static load and put it on the centroid of each slice in a way that is not conducive to slope stability; then, the calculated safety factor calculated using the limit equilibrium method is used as the evaluation index to measure the slope stability under earthquakes. Due to the fact that the vertical seismic load affects both the antisliding force and the sliding force of sliding bodies, and has a small impact on the safety factor, it is usually ignored in the pseudostatic method. The equivalent static load is defined as:

$$F = \frac{aW}{g} = K_c W_i \quad (1)$$

where a is the pseudostatic acceleration, W_i is the weight of slice i, g is the gravitational acceleration constant, and K_c is the seismic coefficient. The key lies in determining the seismic coefficient K_c.

At present, there are many ways to calculate the seismic coefficient K_c. For example, in the Chinese specification, K_c is a constant related to the antiseismic fortification intensity [43]; in the U.S., K_c is a function of the magnitude and the epicenter distance [44]. Hynes-Griffin et al. [45] argued that K_c should be 50% of the peak acceleration of bedrock. Since the Haiyuan earthquake had a magnitude of 8.5, a suggestion of SEED et al. [46] was adopted in this paper when the magnitude was 8.5. The seismic coefficient should be set at 0.15 and the allowable stability safety factor should be 1.15. The Morgenstern–Price method was used to calculate the critical sliding surface and its corresponding safety factor. This method belongs to the classical limit equilibrium method, and its advantage is that the solution process is rigorous and accurate. However, compared to the global method, there may be problems of local convergence or nonconvergence during the iteration process [47]. The safety factor F_S can be calculated iteratively with Equation (2), according to the force balance of the slice [48]:

$$\left(N_i' \tan \varphi_i' + c_i' b_i \sec \alpha_i\right) / F_S = \left(W_i + \lambda f_{i-1} E_{i-1} - \lambda f_i E_i + Q_i \cos \omega_i\right) \sin \alpha_i - \left(-K_c W_i + E_i - E_{i-1} + Q_i \sin \omega_i\right) \cos \alpha_i \quad (2)$$

where N_i' is the normal force acting on slice i, b_i and a_i refer to the width and the inclination of the bottom of slice i, φ_i' is the internal friction angle, c_i' is the cohesion, $\lambda f_i E_i$ and $\lambda f_{i-1} E_{i-1}$ refer to the shear force on both sides of slice i, Q_i is the external force, ω_i is the angle between external force and vertical direction.

2.5. Stability Analysis

Through a statistical analysis of landslide parameters (slope height, slope angle, loess cover thickness) in the field investigations (Figure 8) and by removing individual discrete points, it was found that the original landslide height was centralized in 50–125 m, the original slope angle was centralized in 20–30°, the loess cover thickness was centralized in 10–25 m, and the original landslide slope shape was mainly linear. Therefore, the effect of the slope shape was not considered in this paper.

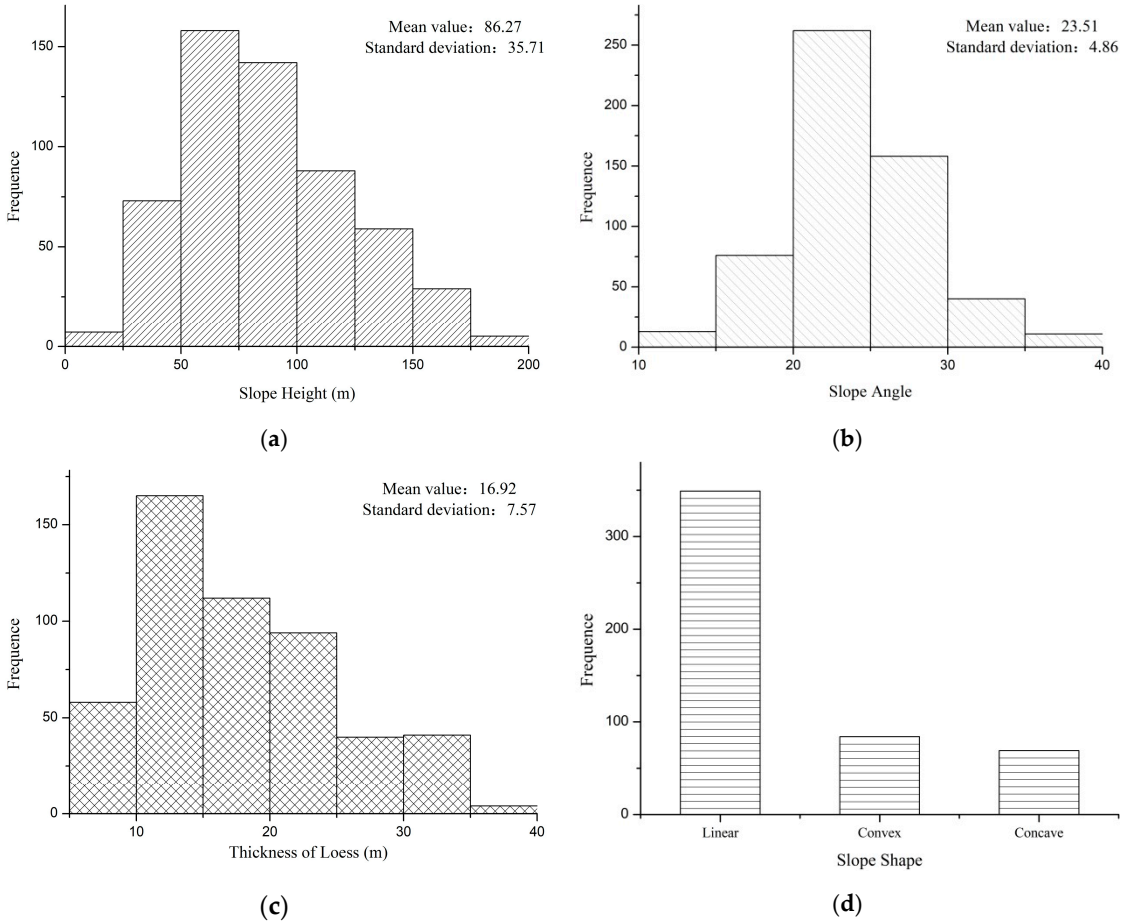
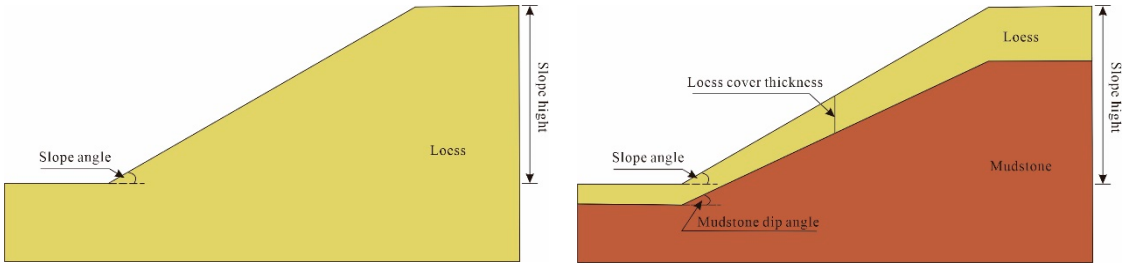


Figure 8. Histograms of landslide topographic parameters: (**a**) histogram of slope height; (**b**) histogram of slope angle; (**c**) histogram of loess cover thickness; (**d**) histogram of slope shape.

According to the statistics and analysis of the above investigation data, four influencing factors, i.e., slope height, slope angle, loess cover thickness, and mudstone dip angle, were determined for evaluating the seismic stability of loess slopes. Two models of a pure loess slope and a loess–mudstone slope was constructed (since the slope angle was not completely the same as the mudstone dip angle, and the effect of the slope shape was ignored, the shape of the mudstone topography and the slope shape were linear; the thickness at half the slope height was taken as the loess cover thickness). The slope geometric model is shown in Figure 9. Using the pseudostatic method, the stability of two slope models with different slope angles and slope heights was calculated. The influence of the existence of the underlying mudstone layer on the loess slope stability was comparatively studied. The loess parameters are shown in Table 1. The underlying mudstone layer was set as the bedrock. The values of all influencing factors are given in Table 2. We mainly used μ as the baseline value for the slope height, slope angle, and loess cover thickness, and $\mu \pm \sigma$ as the value range, where μ is the mean and σ is the standard deviation (as shown in Figure 5). The mudstone dip angle range was determined by referring to the literature [36]; when one factor changed, the baseline values of other factors were adopted.



(**a**) (**b**)

Figure 9. Slope geometric models: (**a**) pure loess slope; (**b**) loess–mudstone slope.

Table 1. Material parameters.

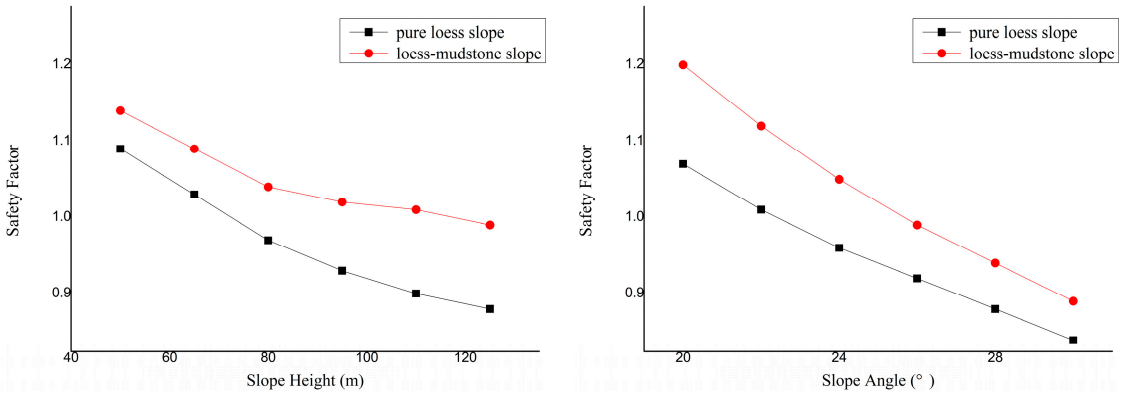
Density (g/cm^3)	Compressibility (MPa^{-1})	Compression Modulus (MPa)	Cohesion (kPa)	Internal Friction Angle (°)
1.63	0.15	12.6	40.88	21.88

Table 2. Value range of influencing factors.

Influencing Factors	Baseline Value	Value Range	Group Distance	Group
Slope height (m)	86	50–125	15	6
Slope angle (°)	24	20–30°	2	6
Loess cover thickness (m)	17	10–25	3	6
Mudstone dip angle (°)	25	25–30°	1	6

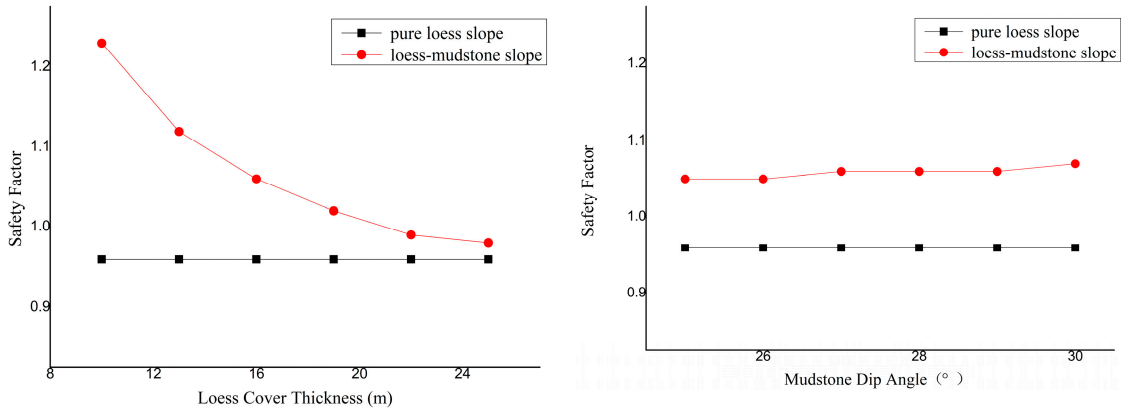
3. Results

The calculation results of the safety factors for two types of slopes are shown in Figure 10. It can be seen that under the same seismic load, the loess–mudstone slope stability was generally higher than that of the pure loess slope, indicating that with the existence of an underlying mudstone layer, the seismic stability of the loess slope was higher. With the increase in the slope height and angle, the seismic stability of both slopes decreased. The thicker the loess cover, the lower the loess–mudstone slope seismic stability. With the increase in the mudstone dip angle, the loess–mudstone slope seismic stability increased. In addition, as can be seen from Figure 10c, as the thickness of loess increased, the safety factor variation curves of the two slope models had an intersection trend. After the calculation, when the loess cover thickness exceeded 33 m, the safety factors of the two slope models were consistent, indicating that there was a critical value for the loess cover thickness. When the loess cover thickness exceeded the critical value, it did not have a significant impact on the seismic stability of the loess–mudstone slope.



(**a**) (**b**)

Figure 10. *Cont.*



(**c**) (**d**)

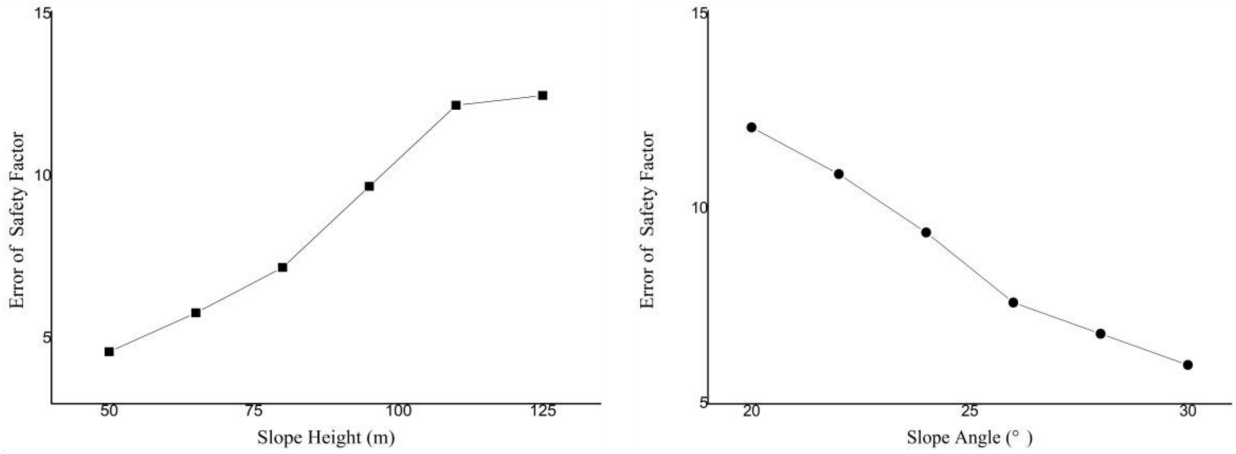
Figure 10. Comparison of safety factors between pure loess slope and loess–mudstone slope: (**a**) relationship between slope height and safety factor; (**b**) relationship between slope angle and safety factor; (**c**) relationship between loess cover thickness and safety factor; (**d**) relationship between mudstone dip angle and safety factor.

The error of safety factor between the two kinds of slopes was defined as:

$$Error = \frac{F_{SLM} - F_{SPL}}{F_{SPL}} \times 100\% \quad (3)$$

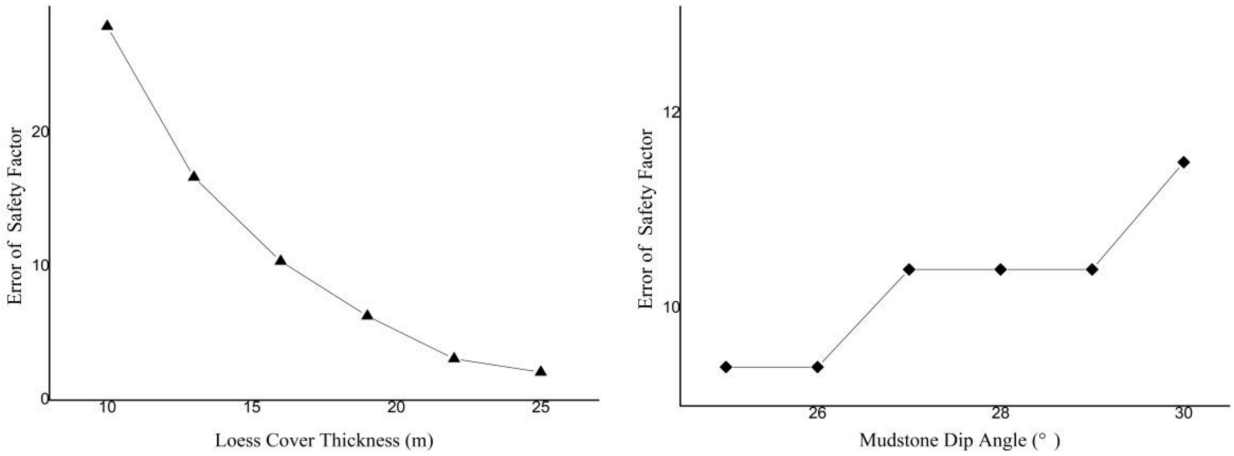
where F_{SLM} is the safety factor of the loess–mudstone slope and F_{SPL} is the corresponding safety factor of the pure loess slope. The results are shown in Figure 11. The error distribution ranges of the two slope model safety factors were 4.6–12.5%, 6.0–12.1%, 2.1–28%, and 9.4–11.5%, respectively, with the variation in slope height, slope angle, loess cover thickness, and mudstone dip angle. It can also be seen that the existence of underlying strata had a significant impact on the seismic stability of the loess slope.

The error of the two kinds of slope safety factors was proportional to the slope height. The error was largest when the slope height was 125 m, reaching 12.5%. The error was inversely proportional to the slope angle; when the slope angle was 20°, the error was largest, reaching 12.1%.



(**a**) (**b**)

Figure 11. *Cont.*



(**c**) (**d**)

Figure 11. Error of safety factors between pure loess slope and loess–mudstone slope: (**a**) relationship between slope height and error of safety factor; (**b**) relationship between slope angle and error of safety factor; (**c**) relationship between loess cover thickness and error of safety factor; (**d**) relationship between mudstone dip angle and error of safety factor.

Compared with the pure loess slope with the same slope height and slope angle, the error of the two kinds of slope safety factors gradually decreased with the increase in the loess cover thickness. When the loess cover thickness was 10 m, the error was largest, that is, 28%. When the mudstone dip angle increased, the error tended to increase. When the mudstone dip angle was 30°, the error was largest (11.5%).

4. Discussion

From the above, it can be seen that the strata structure had a significant impact on the seismic stability of the loess slopes. In this paper, four strata factors, namely, slope height, slope angle, loess cover thickness, and mudstone dip angle, were considered. The impact of these factors on the seismic stability of the loess–mudstone slopes was not entirely the same; if each factor was fully considered in the seismic design of the loess–mudstone slopes, the workload would have been large. Therefore, a sensitivity analysis of these stratal factors that affected the seismic stability of loess–mudstone slopes could classify the degree of influence of each factor and determine the key factor.

There are many methods of conducting a sensitivity analysis, and Huang [49] and Qiu et al. [50] summarized the sensitivity analysis methods of influencing factors of slope stability. The sensitivity of strata factors on the seismic stability of a loess–mudstone slope based on the orthogonal test was studied in this paper. The orthogonal test is a scientific method of studying the sensitivity of multiple factors. This method uses an orthogonal table as a tool to arrange a scheme and analyze its result, so as to find the optimal-level combination of various factors; it can not only reflect the influence of many factors, but also reduce the workload as much as possible on the premise of ensuring the calculation results. The distribution range of each strata factor is shown in Table 3 and varied at equal intervals within their respective intervals. It was a four-factor and four-level test. The orthogonal test was selected as L_{16} (4^4). The pseudostatic method was used to carry out the orthogonal test with safety factors.

Table 3. Orthogonal experiment.

Test Number	Loess Cover Thickness (m)	Mudstone Dip Angle (°)	Slope Angle (°)	Slope Height (m)	Safety Factor
1	10	25	20	50	1.48
2	10	26.7	23.3	75	1.28
3	10	28.4	26.7	100	1.14
4	10	30	30	125	1.03
5	15	25	23.3	100	1.09
6	15	26.7	20	125	1.15
7	15	28.4	30	50	1.02
8	15	30	26.7	75	1.05
9	20	25	26.7	125	0.90
10	20	26.7	30	100	0.84
11	20	28.4	20	75	1.21
12	20	30	23.3	50	1.17
13	25	25	30	75	0.88
14	25	26.7	26.7	50	1.06
15	25	28.4	23.3	125	0.98
16	25	30	20	100	1.11

For the above orthogonal test results, the range analysis method was used to compare the sensitivity of different influencing factors. The analysis results are shown in Table 4. K_i represents the sum of the response values corresponding to the level combination of all factors when a factor was at the i_{th} level; R_j represents the range of factor j, and its value reflects the influence of factor j on the research object. The expression was:

$$\mathrm{R}_j = \max\left\{\overline{\mathrm{K}_1}, \overline{\mathrm{K}_2}, \overline{\mathrm{K}_3}, \overline{\mathrm{K}_4}\right\} - \min\left\{\overline{\mathrm{K}_1}, \overline{\mathrm{K}_2}, \overline{\mathrm{K}_3}, \overline{\mathrm{K}_4}\right\} \quad (4)$$

where $\overline{\mathrm{K}_i}$ is the average value corresponding to K_i.

Table 4. Range analysis of orthogonal experiment.

Parameter	Loess Cover Thickness (m)	Mudstone Dip Angle (°)	Slope Angle (°)	Slope Height (m)
K_1	4.93	4.35	4.95	4.73
K_2	4.31	4.33	4.52	4.42
K_3	4.12	4.35	4.15	4.18
K_4	4.03	4.36	3.77	4.06
R	0.22	0.01	0.29	0.17

It can be seen from Table 4 that the sensitivity influence of the above four factors on slope stability, from high to low, was the slope angle, loess cover thickness, slope height, and mudstone dip angle. Figure 12 shows the factor average in each level. It can be seen that, in addition to the mudstone dip angle, of which the best level was the fourth level, the other three factors were the best at the first level. In conclusion, for the loess–mudstone slope stability in the area affected by the Haiyuan earthquake, the optimum combination was a loess cover thickness of 10 m, a mudstone dip angle of 30°, a slope angle of 20°, and a slope height of 50 m.

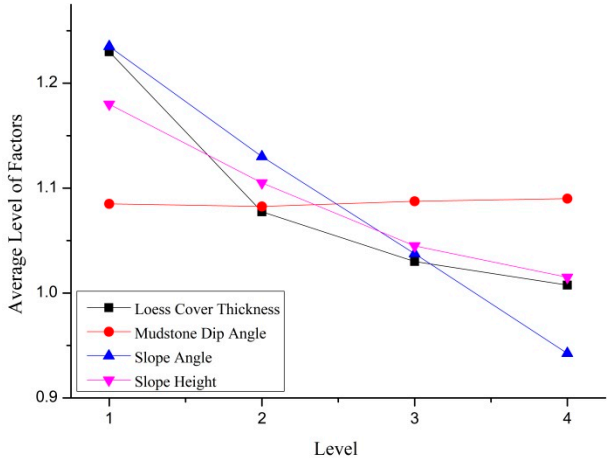


Figure 12. Average value chart of each level of factors.

5. Conclusions

In this paper, the influence of the strata structure on the seismic stability of a loess slope under a given seismic load was studied through field investigations, geotechnical tests, and the pseudostatic method, and the sensitivity degree of the strata factors affecting the loess–mudstone slope seismic stability was analyzed using the orthogonal test and a range analysis.

The conclusions drawn from this study were as follows:

(1) Under the same seismic load, the seismic stability of the loess slope increased when considering the influence of the underlying mudstone strata. With the variation in the four factors affecting the strata structure, the maximum error in the safety factor between the loess mudstone slope and the loess slope reached 28%, indicating that the loess–mudstone strata structure had a significant impact on the seismic stability of the loess slope.

(2) According to the sensitivity analysis results, it is recommended that the influence of the strata structure on the seismic stability of slopes should be considered in the slope survey and design involved in the site selection of projects in high-intensity loess areas, especially the magnitude and level of the slope angle. Secondly, the impact of the loess cover thickness and the slope height should be considered, while the mudstone dip angle had the smallest impact on the seismic stability of the slopes.

Note: In this paper, the pseudostatic method was used to analyze the seismic stability of slopes. Although this method has the characteristics of clear concepts and can provide evaluation indicators of physical significance, its disadvantage is that it ignores the influence of the time and frequency characteristics of the ground motion. In addition, the models established were all two-dimensional dry slope models, without considering the impact of the water table, soil saturation, and cross-section. These issues should be explored in future research works.

Author Contributions: Conceptualization, Z.Z. (Zhaopeng Zhang); methodology, Z.Z. (Zhaopeng Zhang); investigation, Z.Z. (Zhaopeng Zhang); data curation, Z.Z. (Zhiyi Zhao); writing—original draft preparation, Z.Z. (Zhaopeng Zhang); writing—review and editing, W.Q.; supervision, T.Z. All authors have read and agreed to the published version of the manuscript.

Funding: This research was funded by the support of the Scientific Research Fund of the Institute of Engineering Mechanics, China Earthquake Administration (grant no. 2021D24); the Fundamental Research Program of Shanxi Province (grant no. 202203021212119), (grant no. 202103021223211), and (grant no. 202203021212133); the Ningxia Natural Science Foundation Project (grant no. 2021AAC03486).

Institutional Review Board Statement: Not applicable.

Informed Consent Statement: Not applicable.

Data Availability Statement: The data used to support the findings of this study are included within the article.

Acknowledgments: Authors acknowledge the support of Bo Jingshan's team in the creation of this paper.

Conflicts of Interest: The authors declare no conflict of interest.

References

1. Liu, D.S. *Loess and Environment*; Science Press: Beijing, China, 1985.
2. Smalley, I. Landslides in the Thick Loess Terrain of North-West China. *Eng. Geol. Amst.* **2001**, *59*, 201–202. [CrossRef]
3. Wang, L.M.; Wu, Z.J. Earthquake damage characteristics of the minxian-zhangxian Ms 6.6 earthquake and its lessons. *China Earthq. Eng. J.* **2013**, *35*, 401–412.
4. Close, U.; McCormick, E. Where the mountains walked. *Natl. Geogr. Mag.* **1922**, *41*, 445–464.
5. Keefer, D.K. Landslides caused by earthquakes. *Geol. Soc. Am. Bull.* **1984**, *95*, 406–421. [CrossRef]
6. Ishihara, K.; Okusa, S.; Oyagi, N.; Ischuk, A. Liquefaction-induced flow slide in the coll- apsible loess deposit in soviet Tajik. *Soils Found.* **1990**, *30*, 73–89. [CrossRef] [PubMed]
7. Chen, Y.M.; Shi, Y.C. Basic characteristics of seismic landslides in loess area of Northwest China. *J. Seismol. Res.* **2006**, *29*, 276–280.
8. Chang, C.; Yang, S.; Jiao, C.; Peng, D. Sliding distance Statistics and Prediction of the Loess LandslideTriggered by the 1920 Haiyuan Earthquake. *J. Inst. Disaster Prev.* **2019**, *21*, 36–43.
9. Aksoy, B.; Ercanoglu, M. Landslide identification and classification by object-based image analysis and fuzzy logic: An example from the Azdavay region (Kastamonu, Turkey)—ScienceDirect. *Comput. Geosci.* **2012**, *38*, 87–98. [CrossRef]
10. Sato, H.P.; Hasegawa, H.; Fujiwara, S.; Tobita, M.; Koarai, M.; Une, H.; Iwahashi, J. Interpretation of landslide distribution triggered by the 2005 Northern Pakistan earthquake using SPOT 5 imagery. *Landslides* **2007**, *4*, 113–122. [CrossRef]
11. Gorum, T.; Fan, X.; van Westen, C.J.; Huang, R.Q.; Xu, Q.; Tang, C.; Wang, G. Distribution pattern of earthquake-induced landslides triggered by the 12 May 2008 Wenchuan earthquake. *Geomorphology* **2011**, *133*, 152–167. [CrossRef]
12. Zhang, Y.; Xu, Y.R.; Du, P.; Li, W.; Chen, L.; Tian, Q. The Volume Calculation Method of Rock Collapses and Loess Landslides Triggered by the 1556 AD Huaxian M81/2 Earthquake in Shaanxi Province, China. *Earthq. Res. China* **2020**, *34*, 599–616.
13. Chang, C.; Yang, S.; Bo, J.; Duan, Y.; Qiao, F. A satellite image recognition method for loess seismic landslides. *China Earthq. Eng. J.* **2022**, *4*, 811–818.
14. Lan, J.Y.; Bo, J.S.; Li, Y.D.; Zhang, M. Study of large-scale triaxial test of sandy pebble soil and its application to the slope topography effect. *Earthq. Eng. Eng. Dyn.* **2016**, *36*, 157–163.
15. Puri, V.K. *Liquefaction Behavior and Dynamic Properties of Loessial(Silty) Soils*; University of Missouri-Rolla: Rolla, MO, USA, 1984.
16. Prakash, S.; Puri, V.K. Liquefaction of loessial soils. In Proceedings of the Third International Conference on Seismic Microzonation, Seattle, DC, USA, June 28–July 1 1982; Volume 2, pp. 1101–1107.
17. Shannon, S. *Liquefaction and Settlement Characteristics of Silt Soils*; University of Missouri-Rolla: Rolla, MO, USA, 1989.
18. Zhang, Z.; Wang, T.; Wu, S.; Tang, H.; Liang, C. Dynamics characteristic of red clay in a deep-seated landslide, Northwest China: An experiment study. *Eng. Geol.* **2018**, *239*, 254–268. [CrossRef]
19. Guo, J.Y.; Li, R.J.; Zhang, X.Z. Analysis on Influence of Earthquake Motion to Loess Slope Stability. *Adv. Mater. Res.* **2011**, *243–249*, 5157–5160. [CrossRef]
20. Yin, X.; Wang, L. Shaking Table Tests on Sliding Displacements of Loess Slope under Coupling Effect of Rainfall and Earthquake. *Shock Vib.* **2019**, *2019*, 5736305. [CrossRef]
21. Pu, X.W.; Wan, L.M.; Wang, P. Initiation mechanism of mudflow-like loess landslide induced by the combined effect of earthquakes and rainfall. *Nat. Hazards* **2021**, *105*, 3079–3097. [CrossRef]
22. Wu, Z.J.; Zhao, D.Y.; Che, A.L.; Chen, D.W.; Liang, C. Dynamic response characteristics and failure mode of slopes on the loess tableland using a shaking-table model test. *Landslides* **2020**, *17*, 1561–1575. [CrossRef]
23. Zhang, Z.; Wang, T.; Wu, S.; Tang, H.; Liang, C. Seismic performance of loess-mudstone slope in Tianshui—Centrifuge model tests and numerical analysis. *Eng. Geol.* **2017**, *222*, 225–235. [CrossRef]
24. Huang, Q.; Jia, X.; Peng, J.; Liu, Y.; Wang, T. Seismic response of loess-mudstone slope with bedding fault zone. *Soil Dyn. Earthq. Eng.* **2019**, *123*, 371–380. [CrossRef]
25. Wang, Z.; Ni, W.; Jiang, Q.; Xu, L. Dynamic Deformation Analysis of Seismic Loess Landslide covered on Mud Rock. *J. Catastrophology* **2018**, *33*, 225–229.
26. Chen, J.; Wang, L.; Wang, P.; Che, A. Failure mechanism investigation on loess–mudstone landslides based on the Hilbert–Huang transform method using a large-scale shaking table test. *Eng. Geol.* **2022**, *302*, 106630. [CrossRef]
27. Chang, C.; Bo, J.; Qi, W.; Qiao, F.; Peng, D. Study on instability and damage of a loess slope under strong ground motion by numerical simulation. *Soil Dyn. Earthq. Eng.* **2022**, *152*, 107050. [CrossRef]
28. Jia, W.L.; Chang, C.Y.; Li, P.R.; Zhang, Z.W.; Xu, J.H.; Yang, J.Y. Numerical simulation of earthquake-induced loess landslides based on particle flow method. *Acta Seismol. Sin.* **2022**, *44*, 677–687.
29. Xu, Y.; Liu-Zeng, J.; Allen, M.B.; Zhang, W.; Du, P. Landslides of the 1920 Haiyuan earthquake, northern China. *Landslides* **2021**, *18*, 935–953. [CrossRef]

30. Derbyshire, E. Geological hazards in loess terrain, with particular reference to the loess regions of China. *Earth Sci. Rev.* **2011**, *54*, 231–260. [CrossRef]
31. Weng, W.H. *Summary Report on the Investigation of the Gansu Earthquake*; Haiyuan Earthquake Museum: Ningxia, China, 1922.
32. Wang, L.M.; Pu, X.W.; Wu, Z.J.; Xu, X.; Liu, K. Shaking table tests on dynamic response of loess slopes under coupling effects of earthquakes and rainfalls. *Chin. J. Geotech. Eng.* **2018**, *40*, 1287–1293.
33. Zou, J.C.; Shao, S.M. Characteristics of Haiyuan earthquake landslide and its distribution. *Inland Earthq.* **1996**, *10*, 1–6.
34. Li, W.L.; Huang, R.Q.; Pei, X.J.; Zhang, X.C. Historical co-seismic landslide inventory with Google Earth: A case study of 1920 M8.5 Haiyuan Earthquake, China. In *Engineering Geology for Society and Territory*; Springer International Publishing: Berlin/Heidelberg, Germany, 2015; Volume 2, pp. 709–712.
35. Zhuang, J.Q.; Peng, J.B.; Xu, C.; Li, Z.; Densmore, A.; Milledge, D.; Iqbal, J.; Cui, Y. Distribution and characteristics of loess landslides triggered by the 1920 Haiyuan Earthquake, Northwest of China. *Geomorphology* **2018**, *314*, 1–12. [CrossRef]
36. Wu, X.H.; Ni, W.K. *Detailed Investigation Report on Geological Hazards in Xiji County, Ningxia Hui Autonomous Region*; Ningxia Hui Autonomous Region Land and resources investigation and Monitoring Institute: Ningxia, China, 2011.
37. Swan, G.; Cook, J.; Bruce, S.; Meehan, R. Strain rate effects in Kimmeridge Bay shale. *Int. J. Rock Mech. Min. Sci. Geomech. Abstr.* **1989**, *26*, 135–149. [CrossRef]
38. Maqsood, Z.; Koseki, J.; Miyashita, Y.; Xie, J.; Kyokawa, H. Experimental study on the mechanical behaviour of bounded geomaterials under creep and cyclic loading considering effects of instantaneous strain rates. *Eng. Geol.* **2020**, *276*, 105774. [CrossRef]
39. *GB 50123–2019*; Ministry of Housing and Urban-Rural Construction of the People's Republic of China, Standards for Geotechnical Testing Method. China Architecture & Building Press: Beijing, China, 2013.
40. Terzaghi, K. *Mechanisms of Landslides, Engineering Geology (Berdey) Volume*; Geological Society of America: Boulder, CO, USA, 1950.
41. Baker, R.; Shukha, R.; Operstein, V.; Frydman, S. Stability Charts for Pseudo—Static Slope Stability Analysis. *Soil Dyn. Earthq. Eng.* **2006**, *26*, 813–823. [CrossRef]
42. Yang, X.G.; Chi, S.C. Seismic Stability of Earth—Rock Dams Using Finite Element Limit Analysis. *Soil Dyn. Earthq. Eng.* **2014**, *64*, 1–10. [CrossRef]
43. *GB 50330-2013*; Ministry of Housing and Urban-Rural Construction of the People's Republic of China, Technical Code for Building Slope Engineering. Architecture & Building Press: Beijing, China, 2013.
44. California Geological Survey (CGS). *Guidelines for Evaluating and Mitigating Seismic Hazards in California*; Special Publication 117A; CGS: Sacramento, CA, USA, 2008.
45. Hynes-Griffin, M.E.; Franklin, A.G. *Rationalizing the Seismic Coefficient Method*; Department of the Army Waterways Experiment Station Corps of Engineers: Vicksburg, MS, USA, 1984.
46. Seed, H.B. Considerations in the Earthquake Resistant Design of Earth and Rockfill Dams. *Geotechnique* **1979**, *29*, 215–263. [CrossRef]
47. Zhang, T.; Zheng, H.; Sun, G. Global method for stability analysis of anchored slopes. *Int. J. Numer. Anal. Methods Geomech.* **2019**, *43*, 124–137. [CrossRef]
48. Morgenstern, N.R.; Price, V.E. The analysis of the stability of general slip surfaces. *Geotechnique* **1965**, *15*, 79–93. [CrossRef]
49. Huang, A.P. *Sensitivity Analysis of Factors Affecting the Stability of High Fill Slope*; Lanzhou University of Technology: Lanzhou, China, 2020.
50. Qiu, H.J.; Zhu, Y.R.; Zhou, W.P.; Sun, H.S. Influence of DEM resolution on landslide simulation performance based on the Scoops3D model. *Geomat. Nat. Hazards Risk* **2022**, *13*, 1663–1681. [CrossRef]

Disclaimer/Publisher's Note: The statements, opinions and data contained in all publications are solely those of the individual author(s) and contributor(s) and not of MDPI and/or the editor(s). MDPI and/or the editor(s) disclaim responsibility for any injury to people or property resulting from any ideas, methods, instructions or products referred to in the content.